

Posterior-Mean Denoising Diffusion Model for Realistic PET Image Reconstruction

Yiran Sun^{1,2} and Osama Mawlawi^{2,1}

¹Department of Electrical and Computer Engineering, Rice University.

²Department of Imaging Physics, UT MD Anderson Cancer Center.

Abstract

Positron Emission Tomography (PET) is a functional imaging modality that enables the visualization of biochemical and physiological processes across various tissues. Recently, deep learning (DL)-based methods have demonstrated significant progress in directly mapping sinograms to PET images. However, regression-based DL models often yield overly smoothed reconstructions lacking of details (i.e., low distortion, low perceptual quality), whereas GAN-based and likelihood-based posterior sampling models tend to introduce undesirable artifacts in predictions (i.e., high distortion, high perceptual quality), limiting their clinical applicability. To achieve a robust perception-distortion tradeoff, we propose *Posterior-Mean Denoising Diffusion Model* (PMDM-PET), a novel approach that builds upon a recently established mathematical theory to explore the closed-form expression of perception-distortion function in diffusion model space for PET image reconstruction from sinograms. Specifically, PMDM-PET first obtained posterior-mean PET predictions under minimum mean square error (MSE), then optimally transports the distribution of them to the ground-truth PET images distribution. Experimental results demonstrate that PMDM-PET not only generates realistic PET images with possible minimum distortion and optimal perceptual quality but also outperforms five recent state-of-the-art (SOTA) DL baselines in both qualitative visual inspection and quantitative pixel-wise metrics PSNR (dB)/SSIM/NRMSE.

Keywords: Deep Learning, Image Reconstruction, PET

1 Introduction

Positron Emission Tomography (PET) is a functional imaging modality that visualizes biochemical and physiological processes across tissues. During acquisition, high-energy photons from positron annihilation are detected by ring-structured arrays within a PET scanner. Photon counts from multiple angles are compiled into projections and arranged into sinograms, forming the basis for PET image reconstruction [1]. Over the past few decades, various approaches have been developed to reconstruct high-quality PET images from sinograms, broadly categorized into four main directions: 1) Traditional analytical methods, such as filtered back-projection (FBP); 2) Iterative techniques, including ordered subsets expectation maximization (OSEM), maximum-likelihood expectation maximization (MLEM) [2, 3], and penalized log-likelihood (PLL) methods [4, 5]; 3) Deep learning-based approaches [6–13]; 4) Compressed sensing-based methods [14, 15]. Some of these methods have several limitations, for example, traditional analytical approaches are highly sensitive to noise and prone to streak artifacts, iterative methods often suffer from high computational complexity, and compressed sensing techniques rely heavily on the choice of sparsifying transforms and regularization terms.

In this study, we focus on supervised deep learning (DL) methods that directly map sinograms to PET images, as they effectively model complex nonlinear relationships without being constrained by external physical factors. However, regression-based DL approaches trained with mean square error (MSE) often produce overly smooth textures and suboptimal perceptual quality (i.e., low distortion, low perceptual quality) [16, 17]. To improve the perceptual quality in reconstructed images, conditional generative models (cGMs) have emerged as a promising posterior sampling approach, which incorporates novel loss terms to capture underlying posterior distributions and generate realistic images from corresponding measurements. However, cGMs present significant challenges: generative adversarial networks (GANs) [18] often suffer from non-convergence and mode collapse due to their adversarial training process, which may introduce numerous artifacts in predictions [19]; variational autoencoders (VAEs) [20] struggle with balancing reconstruction fidelity and Kullback–Leibler (KL) divergence, which often results in overly smooth predictions; and denoising diffusion probabilistic models (DDPMs) [21] involves an iterative denoising process during inference, which sometimes leads to high-frequency details loss in predictions. Furthermore, Freirich et al. [22] demonstrated that such posterior sampling alone is not an optimal strategy for achieving a desirable perception-distortion tradeoff. Instead, it can be improved by leveraging an optimal MSE estimator without compromising perceptual quality.

To achieve an optimal tradeoff between distortion and perceptual quality, several studies have explored improved reconstruction techniques that minimize distortion while adhering to a specified perceptual constraint [12, 16, 17, 22–24]. Related theoretical frameworks have mathematically demonstrated that this perception-distortion optimization problem can be addressed by optimally transporting posterior mean predictions to the distribution of ground-truth images [16, 22–24]. Motivated by this insight, we extend this theory to denoising diffusion probabilistic models (DDPMs) and propose *Posterior-Mean Denoising Diffusion Model* (PMDM-PET), a simple yet

effective framework for generating PET images directly from sinograms while achieving both possible minimum distortion and optimal perceptual quality (see Fig. 1). Specifically, we first compute posterior mean PET image predictions under MSE distortion supervision. We then employ a conditional diffusion probabilistic model to optimally transport these mean predictions toward the distribution of ground-truth PET images under evidence lower bound (ELBO)-based perception supervision. To evaluate PMDM-PET, we perform both qualitative and quantitative evaluations in terms of visual inspection and pixel-wise metrics PSNR (dB)/SSIM [25]/NRMSE [26]. Experimental results demonstrate that PMDM-PET not only generates robust and realistic PET images with a favorable perception-distortion tradeoff but also outperforms five recent state-of-the-art (SOTA) deep learning-based baselines.

2 Preliminaries

2.1 Perception-Distortion Tradeoff

Deep learning-based medical image reconstruction approaches are typically evaluated based on two key aspects: (1) the extent to which the reconstructed images $\hat{\mathbf{x}}_0$ approximates the reference image \mathbf{x}_0 on average (distortion quality) and (2) the similarity between the distributions of $\hat{\mathbf{x}}_0$ and \mathbf{x}_0 (perceptual quality). Blau et al. [16] established that distortion and perceptual quality are inherently at odds, where minimizing distortion often comes at the expense of perceptual fidelity, and vice versa (see Fig. 1). To achieve an optimal tradeoff between perception (P) and distortion (D), we formulate the problem as:

$$D(P) = \min_{p_{\hat{\mathbf{x}}_0}} \mathbb{E}[\Delta(\mathbf{x}_0, \hat{\mathbf{x}}_0)] \quad \text{s.t.} \quad d(p_{\mathbf{x}_0}, p_{\hat{\mathbf{x}}_0}) \leq P, \quad (1)$$

where $\Delta(\cdot, \cdot)$ represents a distortion measure, and $d(\cdot, \cdot)$ denotes a divergence between distributions. Specifically, we focus on mean square error (MSE) distortion, defined as $\Delta(\mathbf{x}_0, \hat{\mathbf{x}}_0) = \|\mathbf{x}_0 - \hat{\mathbf{x}}_0\|^2$, and minimize it under a perfect perceptual index constraint ($P = 0$). This allows us to rewrite Eq. (1) as:

$$D(0) = \min_{p_{\hat{\mathbf{x}}_0}} \mathbb{E}[\|\mathbf{x}_0 - \hat{\mathbf{x}}_0\|^2] \quad \text{s.t.} \quad p_{\mathbf{x}_0} = p_{\hat{\mathbf{x}}_0}. \quad (2)$$

Recent studies [23, 24] have shown that the optimal solution to Eq. (2) can be obtained by first predicting an overly smooth posterior mean \mathbf{x}_0^* under a possible minimum MSE (MMSE) and then sampling final predictions $\hat{\mathbf{x}}_0$ from the posterior distribution conditioned on \mathbf{x}_0^* . In this work, we extend this theoretical framework to the current state-of-the-art (SOTA) generative modeling paradigm—denoising diffusion probabilistic models (DDPMs) [21, 27].

2.2 Denoising Diffusion Probabilistic Models

Denoising Diffusion Probabilistic Models (DDPMs) are powerful deep generative algorithms that achieve state-of-the-art performance across various generative tasks [21,

27, 28]. Unconditional DDPMs approximate the true data distribution through two processes: a fixed forward process and a learning-based reverse process. The forward process is a fixed Markov chain that starts with clean samples from the input data distribution $\mathbf{x}_0 \sim q(\mathbf{x}_0)$ and progressively adds Gaussian noise according to a variance schedule $\beta_{1:T}$, where $\beta_t \in (0, 1)$ for all $t \in [1, T]$:

$$q(\mathbf{x}_t|\mathbf{x}_{t-1}) := \mathcal{N}(\mathbf{x}_t; \sqrt{1 - \beta_t}\mathbf{x}_{t-1}, \beta_t\mathbf{I}), \quad (3)$$

For sufficiently large T and a properly selected variance schedule, \mathbf{x}_T approximates an isotropic Gaussian distribution. Notably, Eq. (3) allows \mathbf{x}_t to be expressed in closed form with respect to \mathbf{x}_0 , which enables efficient training. Define $\alpha_t := 1 - \beta_t$ and $\bar{\alpha}_t := \prod_{s=1}^t \alpha_s$, we can directly sample \mathbf{x}_t at any timestep t from $q(\mathbf{x}_t|\mathbf{x}_0) := \mathcal{N}(\mathbf{x}_t; \sqrt{\bar{\alpha}_t}\mathbf{x}_0, (1 - \bar{\alpha}_t)\mathbf{I})$, which is a linear combination of Gaussian noise $\epsilon \sim \mathcal{N}(0, \mathbf{I})$ and the clean images \mathbf{x}_0 , i.e. $\mathbf{x}_t = \sqrt{\bar{\alpha}_t}\mathbf{x}_0 + \sqrt{1 - \bar{\alpha}_t}\epsilon$.

The goal of the learning-based reverse process is to generate clean images $\hat{\mathbf{x}}_0$ from the noisy samples $\mathbf{x}_T \sim \mathcal{N}(0, \mathbf{I})$. The reverse process is defined as a joint Markov chain $p_\theta(\mathbf{x}_{0:T}) := p(\mathbf{x}_T) \prod_{t=1}^T p_\theta(\mathbf{x}_{t-1}|\mathbf{x}_t)$, where $p(\mathbf{x}_T) = \mathcal{N}(\mathbf{x}_T; \mathbf{0}, \mathbf{I})$, and the transition probabilities $p_\theta(\mathbf{x}_{t-1}|\mathbf{x}_t)$ are parameterized as Gaussian distributions with learned mean and variance:

$$p_\theta(\mathbf{x}_{t-1}|\mathbf{x}_t) := \mathcal{N}(\mathbf{x}_{t-1}; \mu_\theta(\mathbf{x}_t, t), \Sigma_\theta(\mathbf{x}_t, t)), \quad (4)$$

Here, θ represents the learnable parameters of the neural network. The mean function can be reparameterized as $\mu_\theta(\mathbf{x}_t, t) = \frac{1}{\sqrt{\alpha_t}} \left(\mathbf{x}_t - \frac{1 - \alpha_t}{\sqrt{1 - \alpha_t}} \epsilon_\theta(\mathbf{x}_t, t) \right)$, where $\epsilon_\theta(\cdot, \cdot)$ predicts the added noise at each time step. The training objective at time step t is:

$$\mathcal{L}_{DDPMs} := \mathbb{E}_{t \sim [1, T], \mathbf{x}_0, \epsilon} [\|\epsilon_t - \epsilon_\theta(\mathbf{x}_t, t)\|^2]. \quad (5)$$

During inference time, starting from Gaussian noise samples \mathbf{x}_T , we iteratively compute $\mathbf{x}_{t-1} = \frac{1}{\sqrt{\alpha_t}} \left(\mathbf{x}_t - \frac{\beta_t}{\sqrt{1 - \alpha_t}} \epsilon_\theta(\mathbf{x}_t, t) \right) + \sigma_t \mathbf{z}$ over T steps to generate clean images $\hat{\mathbf{x}}_0$, where $\mathbf{z} \sim \mathcal{N}(0, \mathbf{I})$.

3 Methods

3.1 Overview

Let s denote the sinogram images, \mathbf{r}_0 the corresponding reference PET images, and $\hat{\mathbf{r}}_0$ the final predicted PET images, where $s, \mathbf{r}_0, \hat{\mathbf{r}}_0 \in \mathbb{R}^{1 \times H \times W}$. In our setup, the input sinogram images s and their corresponding PET images \mathbf{r}_0 are padded to dimensions of $1 \times 256 \times 256$. The general objective of this work is to approximate the stochastic transformation $p(\hat{\mathbf{r}}_0|s)$, i.e., $p(\hat{\mathbf{r}}_0|\mathbf{r}_0^*)p(\mathbf{r}_0^*|s)$, where \mathbf{r}_0^* represents posterior mean PET predictions obtained from the estimator with possible MMSE distortion D^* . According to [22], since $\hat{\mathbf{r}}_0$ is independent of \mathbf{r}_0 given s , the total expected distortion then can

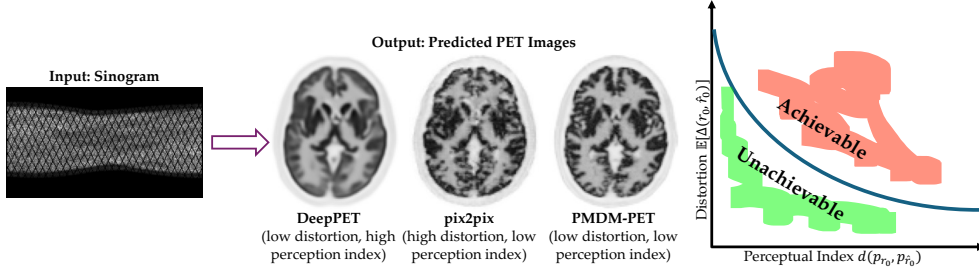


Fig. 1 Perception-Distortion Tradeoff in PET Image Reconstruction from Sinogram. Regression-based DeepPET [6] achieves a low distortion quality but produces blurry predictions, while posterior sampling from pix2pix [29] has good perceptual quality but introduce numerous artifacts. Our proposed PMDM-PET generates robust predictions by achieving a high distortion and perception quality at the same time. Specifically, PMDM-PET explores the perception-distortion function (right) in terms of MSE distortion and ELBO-Based (KL divergence) perception index.

be decomposed as:

$$\mathbb{E}[\|\mathbf{r}_0 - \hat{\mathbf{r}}_0\|^2] = \mathbb{E}[\|\mathbf{r}_0 - \mathbf{r}_0^*\|^2] + \mathbb{E}[\|\mathbf{r}_0^* - \hat{\mathbf{r}}_0\|^2], \quad (6)$$

In this work, we optimize the distortion-perception function within the diffusion probabilistic model framework. Then Eq. (2) and (6) can be reformulated as:

$$D(0) = D^* + \min_{p_{\hat{\mathbf{r}}_0} p_{\mathbf{r}_0^*}} \left\{ \sum_{t=1}^T \text{KL}(q(\hat{\mathbf{r}}_t | \hat{\mathbf{r}}_0, \mathbf{r}_0^*) \parallel p_{\theta}(\hat{\mathbf{r}}_t | \hat{\mathbf{r}}_{t+1}, \mathbf{r}_0^*)) : p_{\hat{\mathbf{r}}_0} p_{\mathbf{r}_0^*} \in \mathcal{M}(p_{\mathbf{r}_0}, p_{\mathbf{r}_0^*}) \right\}. \quad (7)$$

where $\mathcal{M}(p_{\mathbf{r}_0}, p_{\mathbf{r}_0^*})$ is the set of all probability distributions on $\mathbb{R}^{n_{\mathbf{r}_0}} \times \mathbb{R}^{n_{\mathbf{r}_0}}$ with marginals $p_{\mathbf{r}_0}$ and $p_{\mathbf{r}_0^*}$. We note that this formulation actually aims to minimize the sum of Kullback–Leibler (KL) divergences over T timesteps between $p_{\mathbf{r}_0}$ and $p_{\mathbf{r}_0^*}$, given an estimator with possible MMSE distortion D^* . Therefore, based on this nature, our proposed method PMDM-PET consists of two stages: 1) train a regression-based DL model to predict the posterior mean PET images \mathbf{r}_0^* by minimizing the MSE between reconstructed and ground-truth images (see Sec. 3.1), 2) train a conditional diffusion model to learn the optimal transport path between the distributions of posterior-mean predictions and ground-truth images (see Sec. 3.2). The following sections provide a detailed description of PMDM-PET.

3.2 MSE Supervised Posterior-Mean Estimator

For consistency in comparison, we adopt DeepPET [6], a convolutional encoder-decoder network, as our MSE-based estimator model f_{θ} for $p(\mathbf{r}_0^* | s)$. The model takes sinograms s as input and outputs overly smoothed posterior mean PET images \mathbf{r}_0^* . The encoder consists of convolutional blocks with a stride of 2, doubling the number of feature maps at each stage. Filter sizes decrease from 7×7 (first two layers) to 5×5 (next two layers) and 3×3 for the remaining layers, producing a final output

of 512 feature maps at a resolution of 32×32 . The decoder progressively upsamples the representation using interpolation, followed by 3×3 convolutions that halve the number of feature maps, batch normalization (BN), and ReLU activations. The full network comprises 22 convolutional layers. Alternative neural network designs may achieve comparable performance. The estimator f_θ is trained end-to-end under MSE supervision on sinogram-PET pairs:

$$\mathcal{L}_{DeepPET} := \mathbb{E} [\|\mathbf{r}_0 - f_\theta(s)\|^2]. \quad (8)$$

The possible MMSE distortion D^* is then attained by predicting posterior mean PET images \mathbf{r}_0^* from the trained estimator model $f_{\theta^*}(s)$.

3.3 Posterior-Mean Denoising Diffusion Model

Following previous Sec. 2.2, PMDM-PET similarly approximates the posterior-mean conditioned distribution $p(\hat{\mathbf{r}}_0|\mathbf{r}_0^*)$ through a fixed forward process and a learning-based reverse process. The deterministic forward process begins with clean PET samples drawn from the input data distribution $\mathbf{r}_0 \sim q(\mathbf{r}_0)$ and \mathbf{r}_t is a linear combination of noise $\epsilon \sim \mathcal{N}(0, \mathbf{I})$ and \mathbf{r}_0 , i.e. $\mathbf{r}_t = \sqrt{\alpha_t}\mathbf{r}_0 + \sqrt{1-\alpha_t}\epsilon$. The goal of the learning-based reverse process is to generate clean PET images $\hat{\mathbf{r}}_0$ from the noisy sample $\mathbf{r}_T \sim \mathcal{N}(0, \mathbf{I})$ given posterior mean PET images \mathbf{r}_0^* , i.e. approximate the optimal transport $p(\hat{\mathbf{r}}_0|\mathbf{r}_0^*)$. This process is modeled using a joint Markov chain $p_\theta(\mathbf{r}_{0:T}) := p(\mathbf{r}_T) \prod_{t=1}^T p_\theta(\mathbf{r}_{t-1}|\mathbf{r}_t, \mathbf{r}_0^*)$, and the transition probabilities are parameterized as $\mathcal{N}(\mathbf{r}_{t-1}; \mu_\theta(\mathbf{r}_t, t, \mathbf{r}_0^*), \Sigma_\theta(\mathbf{r}_t, t, \mathbf{r}_0^*))$, where θ represents the learnable parameters of the neural network. The mean function is further reparameterized as $\mu_\theta(\cdot, \cdot) = \frac{1}{\sqrt{\alpha_t}} \left(\mathbf{r}_t - \frac{1-\alpha_t}{\sqrt{1-\alpha_t}} \epsilon_\theta(\mathbf{r}_t, t, \mathbf{r}_0^*) \right)$, where $\epsilon_\theta(\cdot, \cdot)$ predicts the noise added at each time step.

Align with previous work on diffusion models [21, 30], we utilize a convolutional U-Net for denoising at each step of the reverse process. The posterior mean estimation \mathbf{r}_0^* is incorporated into the denoising process as an additional condition. During training, at each iteration, a batch of random sinogram-PET pairs is sampled, and PMDM-PET is optimized by minimizing the denoising loss (where $\mathbf{r}_0^* = f_{\theta^*}(s)$):

$$\mathcal{L}_{PMDM-PET} := \mathbb{E}_{t \sim [1, T], \mathbf{r}_0, \epsilon} [\|\epsilon_t - \epsilon_\theta(\mathbf{r}_t, t, \mathbf{r}_0^*)\|^2]. \quad (9)$$

During inference time, starting from Gaussian noise sample \mathbf{r}_T , we iteratively compute $\mathbf{r}_{t-1} = \frac{1}{\sqrt{\alpha_t}} \left(\mathbf{r}_t - \frac{\beta_t}{\sqrt{1-\alpha_t}} \epsilon_\theta(\mathbf{r}_t, t, \mathbf{r}_0^*) \right) + \sigma_t \mathbf{z}$ over T steps to generate clean predicted images $\hat{\mathbf{r}}_0$, where $\mathbf{z} \sim \mathcal{N}(0, \mathbf{I})$.

4 Experiments

4.1 Datasets and Preprocessing

We follow the data processing steps and use the code from [9, 31] for sinogram-PET pair data preparation. We simulated 2D ^{18}F -FDG PET images from 20 BrainWeb 3D brain phantoms [32], acquired on a Siemens Biograph mMR scanner with a spatial

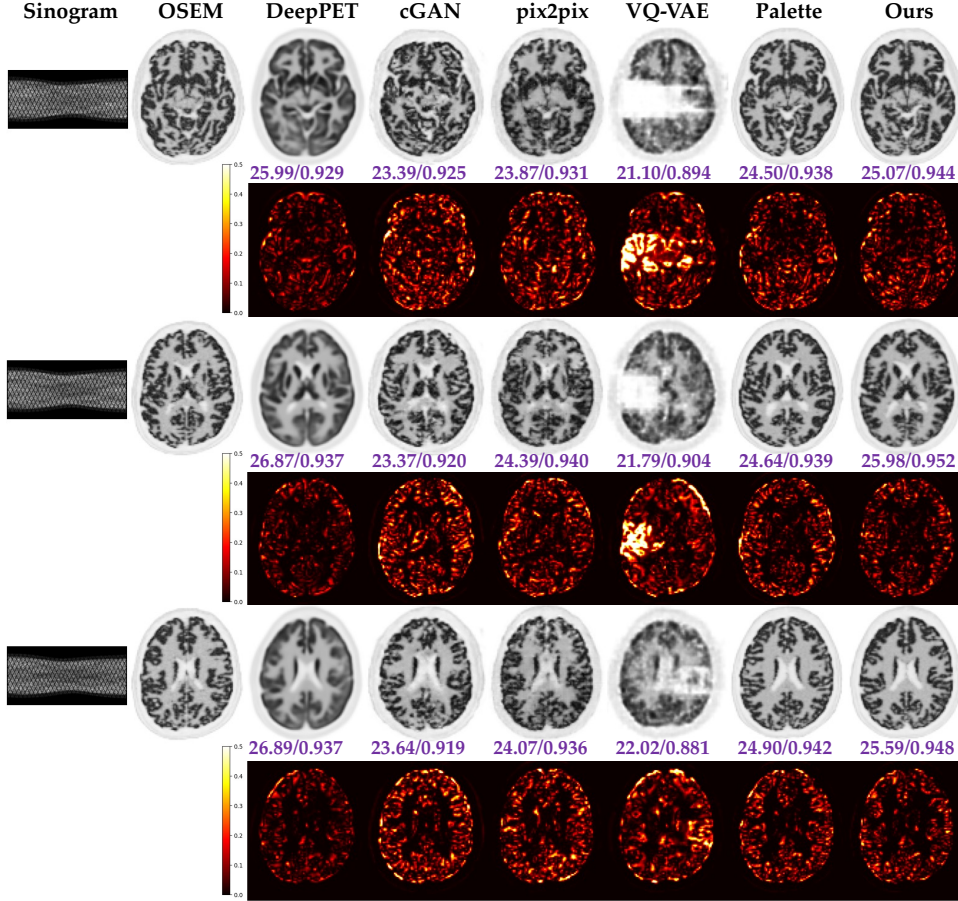


Fig. 2 Qualitative comparison of PMDM-PET with Five Baselines on Three Example Slices. The first column shows the input sinogram images, and the second column shows the reference images reconstructed using OSEM algorithm. The third to seventh columns correspond to the five baselines (labeled above each image), and the final column shows the reconstructed PET images using our proposed PMDM-PET method. PSNR/SSIM values are reported below each slice, and squared error maps between each method and the reference image are also displayed (second, fourth and sixth rows).

resolution of $2.086 \times 2.086 \times 2.031 \text{ mm}^3$ and a matrix size of $344 \times 344 \times 127$. To augment the dataset, each phantom was axially rotated by five random angles in the range $[0, 15]$ degrees, yielding $20 * 5$ 3D brain phantoms. For each phantom, we extracted 55 non-contiguous axial slices and generated their corresponding sinograms using 1×10^{10} counts and point spread function (PSF) modeled with 2.5 mm full-width-at-half-maximum (FWHM) Gaussian kernels. High-count reference PET images were reconstructed using OSEM algorithm with 10 iterations and 14 subsets. The dataset was divided into $17 * 5$ brain phantoms (4675 slices) for training, $1 * 5$ brain phantoms (275 slices) for validation, and $2 * 5$ brain phantoms (550 slices) for testing.

Table 1 Quantitative Evaluation using PSNR (dB)/SSIM/NRMSE. Red and blue indicate the best and second-best results. MParam. denotes the number of trainable parameters of the model.

Type	Model	PSNR \uparrow	SSIM \uparrow	NRMSE \downarrow	MParam.
Regression-based	DeepPET [6]	27.10 \pm 1.01	0.938 \pm 0.007	0.044	11.02
GAN-based	cGAN [34]	22.20 \pm 3.12	0.909 \pm 0.035	0.084	14.13
	pix2pix [29]	22.43 \pm 3.25	0.915 \pm 0.036	0.082	14.13
Likelihood-based	VQ-VAE [35]	20.86 \pm 2.16	0.873 \pm 0.023	0.093	4.87
	Palette [36]	25.40 \pm 1.00	0.945 \pm 0.007	0.054	35.71
	PMDM-PET	26.01 \pm 1.03	0.950 \pm 0.006	0.050	35.71

4.2 Implementation Details

We implemented all experiments using PyTorch [33] on NVIDIA Quadro RTX 8000 GPUs. The MSE estimator (see Sec. 3.1) was trained using the Adam optimizer with a learning rate of 1×10^{-4} and a weight decay of 1×10^{-5} . PMDM-PET was subsequently trained with a learning rate of 3×10^{-5} . Both models were trained for 500 epochs with a batch size of 4. Reconstruction quality was evaluated using metrics: Peak Signal to Noise Ratio (PSNR) [25] and Normalized Root Mean Square Error (NRMSE) [26] for distortion quality, and Structural Similarity Index Measure (SSIM) [25] along with visual inspection for perceptual quality.

4.3 Baselines

We compared the performance of PMDM-PET against five baseline algorithms: DeepPET [6], cGAN [34], pix2pix [29], VQ-VAE [35], and Palette [36]. DeepPET is a regression-based method using a convolutional encoder-decoder to map sinograms to PET images. cGAN is a conditional generative adversarial network for image reconstruction. pix2pix employs a conditional least-squares GAN for image-to-image translation. VQ-VAE combines variational autoencoders with vector quantization to learn discrete latent representations for image generation. Palette is a diffusion model conditioned on sinograms. We used the publicly available implementations for all baselines and trained them to full convergence following the recommended settings.

4.4 Reconstruction Results

We compared the performance of PMDM-PET against five baseline algorithms: DeepPET [6], cGAN [34], pix2pix [29], VQ-VAE [35], and Palette [36]. It is worth noting that DeepPET can be regarded as a model trained without a perceptual constraint and Palette is trained without an MSE estimator, which can also be seen as an ablation study when compared to our PMDM-PET. Table. 1 summarizes the average pixel-wise PSNR (dB)/SSIM/NRMSE values across all reconstructed slices, along with the number of trainable parameters for each method. PMDM-PET achieves a 0.61 dB improvement in PSNR over Palette, demonstrating the effectiveness of incorporating an MMSE estimator to reduce distortion while preserving high perceptual quality.

While DeepPET achieves comparable PSNR values, its reconstructed PET images appear significantly blurrier and less perceptually faithful, as illustrated in Fig. 2. This aligns with the tradeoff theory discussed in Sec. 2.1, where generative models leveraging stochastic posterior sampling sacrifice pixel-wise distortion (resulting in lower PSNR) while maintaining fidelity to the underlying distribution [16, 17]. Additionally, PMDM-PET outperforms cGAN, pix2pix, and VQ-VAE by approximately 3.81 dB, 3.58 dB, and 5.15 dB in PSNR, respectively. Fig. 2 further visualizes reconstruction results, comparing all baseline methods side by side. PMDM-PET produces the most robust reconstructions, excelling in both distortion and perceptual quality. In contrast, cGAN, pix2pix, VQ-VAE, and Palette introduce noticeable artifacts, while DeepPET generates overly smooth reconstructions with unrealistic fine details.

5 Conclusion

We propose *Posterior-Mean Denoising Diffusion Model* (PMDM-PET) to generate PET images directly from sinograms while achieving a favorable balance between distortion and perceptual quality. We evaluate PMDM-PET on simulated human brain data [32] using both qualitative and quantitative metrics. Experimental results demonstrate that PMDM-PET produces highly realistic PET images with an optimal distortion-perception tradeoff and outperforms five recent SOTA DL baselines. Future work will focus on clinical evaluations.

References

- [1] Fahey, F.H.: Data acquisition in pet imaging. *Journal of nuclear medicine technology* **30**(2), 39–49 (2002)
- [2] Hudson, H.M., Larkin, R.S.: Accelerated image reconstruction using ordered subsets of projection data. *IEEE transactions on medical imaging* **13**(4), 601–609 (1994)
- [3] Zhu, Y.-M.: Ordered subset expectation maximization algorithm for positron emission tomographic image reconstruction using belief kernels. *Journal of Medical Imaging* **5**(4), 044005–044005 (2018)
- [4] Wang, G., Qi, J.: Penalized likelihood pet image reconstruction using patch-based edge-preserving regularization. *IEEE transactions on medical imaging* **31**(12), 2194–2204 (2012)
- [5] Zhang, H., Wang, Y., Qi, J., Abbaszadeh, S.: Penalized maximum-likelihood reconstruction for improving limited-angle artifacts in a dedicated head and neck pet system. *Physics in Medicine & Biology* **65**(16), 165016 (2020)
- [6] Häggström, I., Schmidlein, C.R., Campanella, G., Fuchs, T.J.: DeepPET: A deep encoder–decoder network for directly solving the pet image reconstruction inverse problem. *Medical image analysis* **54**, 253–262 (2019)

- [7] Whiteley, W., Luk, W.K., Gregor, J.: Directpet: full-size neural network pet reconstruction from sinogram data. *Journal of Medical Imaging* **7**(3), 032503–032503 (2020)
- [8] Ma, R., Hu, J., Sari, H., Xue, S., Mingels, C., Viscione, M., Kandarpa, V.S.S., Li, W.B., Visvikis, D., Qiu, R., *et al.*: An encoder-decoder network for direct image reconstruction on sinograms of a long axial field of view pet. *European journal of nuclear medicine and molecular imaging* **49**(13), 4464–4477 (2022)
- [9] Hu, R., Liu, H.: Transem: Residual swin-transformer based regularized pet image reconstruction. In: *International Conference on Medical Image Computing and Computer-Assisted Intervention*, pp. 184–193 (2022). Springer
- [10] Singh, I.R., Denker, A., Barbano, R., Kereta, Ž., Jin, B., Thielemans, K., Maass, P., Arridge, S.: Score-based generative models for pet image reconstruction. *arXiv preprint arXiv:2308.14190* (2023)
- [11] Cui, J., Zeng, P., Zeng, X., Wang, P., Wu, X., Zhou, J., Wang, Y., Shen, D.: Trido-former: A triple-domain transformer for direct pet reconstruction from low-dose sinograms. In: *International Conference on Medical Image Computing and Computer-Assisted Intervention*, pp. 184–194 (2023). Springer
- [12] Sun, Y., Diez, V., Mawlawi, O.: R2U-DDPM: A Conditional Diffusion Model with R2U-Net Guidance for Realistic PET Image Synthesis. *Soc Nuclear Med* (2024)
- [13] Sun, Y., Mawlawi, O.: Legopet: Hierarchical feature guided conditional diffusion for pet image reconstruction. *arXiv preprint arXiv:2411.16629* (2024)
- [14] Xie, Y., Li, Q.: A review of deep learning methods for compressed sensing image reconstruction and its medical applications. *Electronics* **11**(4), 586 (2022)
- [15] Malczewski, K.: Pet image reconstruction using compressed sensing. In: *2013 Signal Processing: Algorithms, Architectures, Arrangements, and Applications (SPA)*, pp. 176–181 (2013). IEEE
- [16] Blau, Y., Michaeli, T.: The perception-distortion tradeoff. In: *Proceedings of the IEEE Conference on Computer Vision and Pattern Recognition*, pp. 6228–6237 (2018)
- [17] Ledig, C., Theis, L., Huszár, F., Caballero, J., Cunningham, A., Acosta, A., Aitken, A., Tejani, A., Totz, J., Wang, Z., *et al.*: Photo-realistic single image super-resolution using a generative adversarial network. In: *Proceedings of the IEEE Conference on Computer Vision and Pattern Recognition*, pp. 4681–4690 (2017)
- [18] Goodfellow, I., Pouget-Abadie, J., Mirza, M., Xu, B., Warde-Farley, D., Ozair, S., Courville, A., Bengio, Y.: Generative adversarial networks. *Communications*

of the ACM **63**(11), 139–144 (2020)

- [19] Salimans, T., Goodfellow, I., Zaremba, W., Cheung, V., Radford, A., Chen, X.: Improved techniques for training gans. *Advances in neural information processing systems* **29** (2016)
- [20] Doersch, C.: Tutorial on variational autoencoders. *arXiv preprint arXiv:1606.05908* (2016)
- [21] Ho, J., Jain, A., Abbeel, P.: Denoising diffusion probabilistic models. *Advances in neural information processing systems* **33**, 6840–6851 (2020)
- [22] Freirich, D., Michaeli, T., Meir, R.: A theory of the distortion-perception tradeoff in wasserstein space. *Advances in Neural Information Processing Systems* **34**, 25661–25672 (2021)
- [23] Ohayon, G., Michaeli, T., Elad, M.: Posterior-mean rectified flow: Towards minimum mse photo-realistic image restoration. *arXiv preprint arXiv:2410.00418* (2024)
- [24] Adrai, T., Ohayon, G., Elad, M., Michaeli, T.: Deep optimal transport: A practical algorithm for photo-realistic image restoration. *Advances in Neural Information Processing Systems* **36** (2024)
- [25] Hore, A., Ziou, D.: Image quality metrics: Psnr vs. ssim. In: *2010 20th International Conference on Pattern Recognition*, pp. 2366–2369 (2010). IEEE
- [26] Hyndman, R.J., Koehler, A.B.: Another look at measures of forecast accuracy. *International journal of forecasting* **22**(4), 679–688 (2006)
- [27] Song, Y., Sohl-Dickstein, J., Kingma, D.P., Kumar, A., Ermon, S., Poole, B.: Score-based generative modeling through stochastic differential equations. *arXiv preprint arXiv:2011.13456* (2020)
- [28] Podell, D., English, Z., Lacey, K., Blattmann, A., Dockhorn, T., Müller, J., Penna, J., Rombach, R.: Sdxl: Improving latent diffusion models for high-resolution image synthesis. *arXiv preprint arXiv:2307.01952* (2023)
- [29] Isola, P., Zhu, J.-Y., Zhou, T., Efros, A.A.: Image-to-image translation with conditional adversarial networks. In: *Proceedings of the IEEE Conference on Computer Vision and Pattern Recognition*, pp. 1125–1134 (2017)
- [30] Nichol, A.Q., Dhariwal, P.: Improved denoising diffusion probabilistic models. In: *International Conference on Machine Learning*, pp. 8162–8171 (2021). PMLR
- [31] Mehranian, A., Reader, A.J.: Model-based deep learning pet image reconstruction using forward–backward splitting expectation–maximization. *IEEE transactions on radiation and plasma medical sciences* **5**(1), 54–64 (2020)

- [32] Collins, D.L., Zijdenbos, A.P., Kollokian, V., Sled, J.G., Kabani, N.J., Holmes, C.J., Evans, A.C.: Design and construction of a realistic digital brain phantom. *IEEE transactions on medical imaging* **17**(3), 463–468 (1998)
- [33] Paszke, A., Gross, S., Massa, F., Lerer, A., Bradbury, J., Chanan, G., Killeen, T., Lin, Z., Gimelshein, N., Antiga, L., et al.: Pytorch: An imperative style, high-performance deep learning library. *Advances in neural information processing systems* **32** (2019)
- [34] Mirza, M., Osindero, S.: Conditional generative adversarial nets. arXiv preprint arXiv:1411.1784 (2014)
- [35] Van Den Oord, A., Vinyals, O., et al.: Neural discrete representation learning. *Advances in neural information processing systems* **30** (2017)
- [36] Saharia, C., Chan, W., Chang, H., Lee, C., Ho, J., Salimans, T., Fleet, D., Norouzi, M.: Palette: Image-to-image diffusion models. In: *ACM SIGGRAPH 2022 Conference Proceedings*, pp. 1–10 (2022)